2.3 Linearized formulation of the reconstruction problem

Equation (1) indicates that the detected PA signal is linearly related with the PA source term. Therefore, following linear equation relates the PA signals to the PA sources,

$$\boldsymbol{m} = L\boldsymbol{H}, \tag{3}$$

where $\boldsymbol{m}$ is a MT-vector of the set of PA signals with T time samples measured by M detectors, and $\boldsymbol{H}$ is an N-vector of the PA source spatially discretized into N pixels. L is a $MT \times N$-matrix representing the contributions of the discretized sources to the measured signals. L is obtained by calculating PA signals generated by each of the sources with a unit strength.

Here, we attempt to reconstruct the distribution of μ_a in the medium. So, Eq.(3) is rewritten to relate $\boldsymbol{m}$ and μ_a. We assume that the background absorption, $\bar{\mu}_a$, is given and that $\boldsymbol{H}$ is linear to the perturbation in μ_a, $\Delta\mu_a$ by neglecting the higher order terms,

$$\boldsymbol{H} = \bar{\boldsymbol{H}} + J\Delta\mu_a, \tag{4}$$

where $\bar{\boldsymbol{H}}$ is the light energy absorbed by the background, and $\Delta\mu_a$ is an N-vector of the distribution of the perturbation of μ_a discretized into N pixels. J is the differential coefficients of $\boldsymbol{H}$ at $\bar{\mu}_a$. J has the components of $J_{ii} = \Phi_i + \mu_{a_i} \cdot \partial\Phi_i/\partial\mu_{a_i}$ and $J_{ij} = \mu_{a_i} \cdot \partial\Phi_i/\partial\mu_{a_j}$ for $i \neq j$ where $i, j = 1, 2, \cdots, N$. $\partial\Phi_i/\partial\mu_{a_j}$ is calculated by perturbation method using FEM.

By substituting Eq.(4) to Eq.(2), we obtain following equation,

$$\Delta\boldsymbol{m} = LJ\Delta\mu_a, \tag{5}$$

where $\Delta\boldsymbol{m} = \boldsymbol{m} - L\bar{\boldsymbol{H}}$. From $\Delta\boldsymbol{m}$ which is the PA signals due to the perturbation in μ_a obtained by subtracting the background PA signals from the measured ones, we estimate μ_a distribution as $\hat{\mu}_a = \bar{\mu}_a + \widehat{\Delta\mu}_a$. $\widehat{\Delta\mu}_a$ is reconstructed by the l_p sparsity regularization method or TSVD method in this study.

3. IMAGE RECONSTRUCTION

3.1 l_p sparsity regularization

The reconstruction is achieved by minimizing the squared error between the measured and calculated signals. The measured signals always include measurement noise. Additionally, there exist the mismatches between the forward model constructed with FEM and actual measurement system. The noise and mismatches cause low spatial resolution and artifact in the reconstructed images. To reduce the influence of noise and mismatches, regularization technique is used in the reconstruction process. Then the image reconstruction problem in this study is described as follows,

$$\min_{\Delta\mu_a} \|\Delta\boldsymbol{m} - LJ\Delta\mu_a\|^2 + \lambda \cdot f(\Delta\mu_a), \tag{6}$$

where f is a regularization term and λ is a regularization parameter to adjust the effect of the regularization term on the reconstruction.

The l_p sparsity regularization employs f of the l_p norm of $\Delta\mu_a$,

$$f = \sum_{i=1}^{N} |\Delta\mu_{a_i}|^p, \tag{7}$$

where $0 < p \leq 2$. When $p < 2$, it is problematic to calculate the gradient of f for gradient based non-linear optimization. So, $\Delta\mu_{a_i}$ is expressed by a parameter z_i,[6]

$$\Delta\mu_{a_i} = |z_i|^{2/p} \cdot \mathrm{sgn}(z_i). \tag{8}$$

Then the optimization problem Eq.(6) is rewritten as,

$$\min_{\boldsymbol{z}} \|\Delta\boldsymbol{m} - LJ\Delta\mu_a(\boldsymbol{z})\|^2 + \lambda \cdot \sum_{i=1}^{N} |z_i|^2. \tag{9}$$

By solving the optimization problem in Eq.(9), $\widehat{\Delta\mu}_a$ is reconstructed. It is expected that the l_p sparsity regularization with $p < 2$ provides a sparse solution, and the spatial resolution of the reconstructed image is improved.

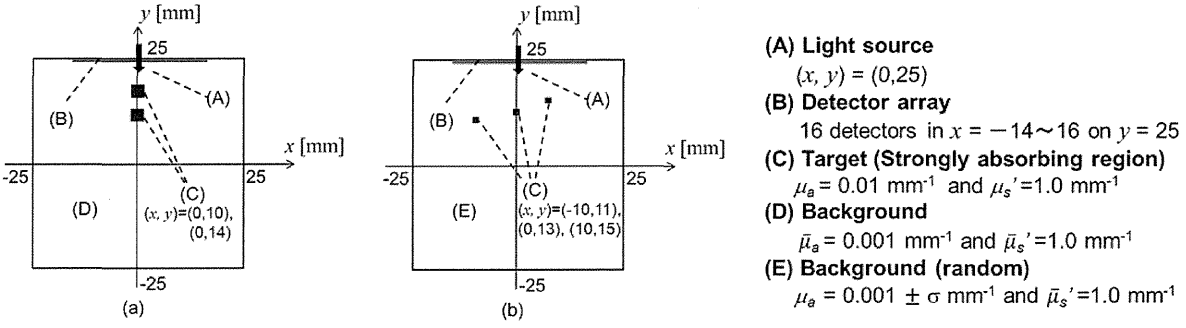

Figure 1. 2D geometries for numerical simulations in cases (a) and (b).

3.2 Truncated singular value decomposition

TSVD method can used to solve Eq.(5). It is well-known that the influences of the noise and of mismatches are amplified by the small singular values of LJ. Thus truncation of the small singular values is effective to stabilize the inverse solution. (LJ) is decomposed as $LJ = V\Lambda W^T$ with the orthogonal matrices of $MT \times MT$-matrix V and $N \times N$-matrix W. Λ is a $MT \times N$-diagonal matrix having the singular values. Then the smaller singular values in Λ are truncated, and inversion matrix $(LJ)^- = W\Lambda^- V^T$ is obtained. Λ^- has the inverse of the singular values. $\widehat{\Delta\mu_a}$ is calculated as,

$$\widehat{\Delta\mu_a} = (LJ)^- \Delta \boldsymbol{m}. \tag{10}$$

The number of the truncated singular values is optimized with generalized cross validation (GCV) method.[9]

4. NUMERICAL SIMULATIONS

4.1 Conditions

4.1.1 Simulation of PA signals

Figure 1 shows 2D geometries used in the numerical simulations. The medium was a square region with 50 mm on a side. The light source was at $(x, y) = (25$ mm, 0 mm), and that 16 ultrasound detectors were placed from $x = -14$ to 16 mm on $y = 25$ mm with an equal spacing of 2 mm. One of the detectors was at the place identical with the light source. We assumed to use the ideal pointwise non-directional detectors.

The light source with a wavelength in NIR range was assumed, and the background medium had uniformly distributed (or mean value of) $\bar{\mu}_s' = 1.0$ mm^{-1} and $\bar{\mu}_a = 0.001$ mm^{-1}. The target, which had μ_a larger than that of the background, was placed in the medium. The positions, sizes and the number of the targets were changed for the purpose of the simulation. We attempted to reconstruct $\hat{\mu}_a$ by the l_p sparsity regularization and TSVD methods.

FEM was used with 10,201 nodes and 20,000 triangular elements to simulate PA signals. The FEM nodes were distributed uniformly with an equal spacing of 0.5 mm. The speed of the PA pressure in the medium of 1500 m/s was used for the FEM calculation, and Grüneissen parameter was set as unity. The time-dependent terms in Eq.(2) were calculated by differential approximation with time step of $\Delta t = 0.1$ μs. Equation (2) discretized by FEM was solved with implicit scheme. The measurement period was assumed as 50 μs. The PA pressure generated by the background $L\bar{H}$ was calculated with the same FEM mesh to simulate $\boldsymbol{m}$. Gaussian noise was added to the simulated $\boldsymbol{m}$. The noise had the standard deviation of 1 % of the maximum of the detected PA signal.

4.1.2 Image reconstruction

We carried out the image reconstruction on pixel basis. The medium was discretized into 625 pixels. Every pixel with 2 mm on a side contained 25 FEM nodes. The centers of the pixels represented the pixel positions, and were

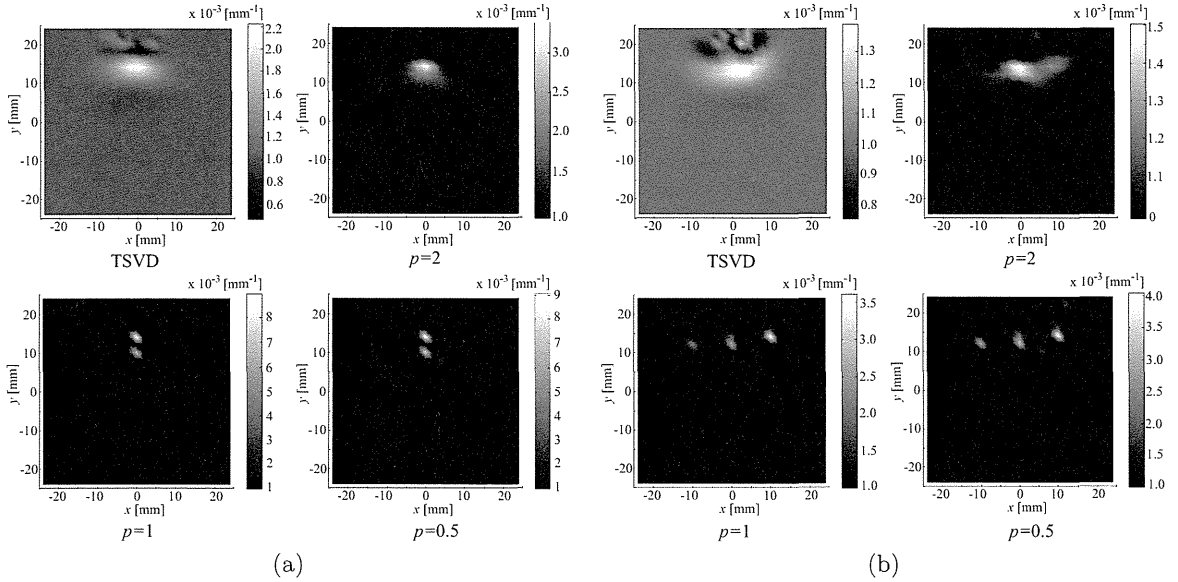

Figure 2. Reconstructed images by TSVD and the l_p sparsity regularization with $p = 2$, 1 and 0.5 in cases (a) and (b).

located at x and y of -24, -22, $\cdots, 22$, 24. The reconstructed $\widehat{\Delta\mu_a}$ were assigned at the centers of the pixels to display the image. The system matrix (LJ) was constructed with the uniform background of $\bar{\mu}_a = 0.01$ mm^{-1} and $\bar{\mu}_s' = 1.0$ mm^{-1}. The simulated $\boldsymbol{m}$ was generated with more precise model of FEM. Therefore, the mismatch between the models for simulating $\boldsymbol{m}$ and for reconstructing images caused the error in the reconstructed image. So, the simulations of the image reconstruction in this study was able to avoid 'inverse crime'.[6]

Equation (9) was solved with non-linear conjugate gradient method. The initial guess of $\Delta\mu_a$ was 1.0×10^{-6} mm^{-1} uniformly. λ was empirically determined. For TSVD, the optimal number of the truncated singular values was searched among the numbers of 0, 10, 20, $\cdots$, and 600 by GCV method. All of the simulations and calculations were done with Matlab (The MathWorks Inc., Natick, Mass., USA).

The simulations for following 2 cases (a) and (b) were carried out to evaluate the performace of the image reconstruction methods. (a) Two targets existed in the medium. The targets had 2 mm on sides and $\mu_a = 0.01$ mm^{-1}. The centers of the targets were at $(x, y) = (0$ mm, 10 mm) and (0 mm, 14 mm) (Fig. 1(a)). Each target fit within a single pixel. (b) There existed three targets in the medium. True μ_a of the targets was 0.01 mm^{-1}. Each target had 1 mm on a side. And the centers of the targets were placed at $(x, y) = (-10$ mm, 11 mm), (0 mm, 13 mm) and (10 mm, 15 mm) (Fig. 1(b)). The centers of the targets were on the boundaries of the pixels and the sizes of the targets were smaller than that of a single pixel. To simulate the variation of the biological tissues in the background, the background μ_a was Gaussian distributed with the standard deviation σ of 10 % of the mean value of $\bar{\mu}_a = 0.001$ mm^{-1}.

4.2 Results and discussions

Figure 2(a) shows the reconstructed images in case (a). The targets were resolved when the l_p sparsity regularization method was used with $p = 0.5$ and 1. TSVD method reconstructed the target robustly, although 2 targets were not resolved. As $p = 2$, the reconstructed target was localized more than the target reconstructed by TSVD. $\widehat{\Delta\mu_a}$ by $p = 2$ became smoother than TSVD. This is the feature of Tikhonov regularization. The maximum PA signal was detected in the detector in the same place with the light source. Therefore, the standard deviation of the noise was much larger than 1 % for the PA signals originated in the targets. When the signal-to-noise ratio is small, noise lowers the spatial resolution of the reconstructed images even though some methods improving the robustness of the reconstruction to noise, such as TSVD and Tikhonov regularization, are used. It is demonstrated that the l_p sparsity regularization with $p < 2$ alleviated the influence of noise and

obtained the high resolution image in noisy situation. The value of $\widehat{\Delta\mu_a}$ with $p = 0.5$ was slightly closer to the true value than that with $p = 1$. In this simulation, the target was localized in the small region. So smaller p provided a better result. But when the true target is not so much localized, small p may reconstruct smaller target than true one. Some criterion to select optimal p is required for reliable reconstruction.

In case of (b), the result was similar to that in case (a). The l_p sparsity regularization with $p < 2$ resolved the targets clearly as shown in Fig.2(b). Besides the true targets were smaller than a single pixel and did not fit within a pixels, the background μ_a to simulate $\boldsymbol{m}$ was not identical to that to reconstruct the image in case (b). This meant that there were mismatches between the forward model for the image reconstruction and the actual measurement conditions. The mismatches affect the reconstruction. Regularization method is effective to reduce the influence of the mismatches in forward modeling. TSVD and the l_p sparsity regularization with $p = 2$ was able to reconstruct the maximum of $\widehat{\Delta\mu_a}$ in one of the positions where the true targets existed. And the $\widehat{\Delta\mu_a}$ distribution indicated a possibility of the existence of the target. On the other hand, the l_p sparsity regularization with $p < 2$ reconstructed well-localized targets. This simulation suggests that once some prior information that indicates the sparse distribution of the target is obtained, the l_p sparsity regularization with $p < 2$ can provide better reconstructed images especially in case where uses of noisy data and of forward model involving some mismatches are necessity.

5. CONCLUSION

The reconstruction of the absorption coefficient with the l_p sparsity regularization method is reported in this paper. The numerical simulations employing FEM compared the reconstructed images with TSVD method and verified that the l_p sparsity regularization method with $p < 2$ reconstructs localized target with high resolution. The reconstruction method is robust to noise and mismatches in the forward modeling. For further development of the PA imaging, improvement of the PA measurement instrument is essential. And the precision of the forward model to be used in the reconstruction is important. The l_p sparsity regularization method will also make contributions to the PA imaging.

REFERENCES

[1] L. V. Wang and S. Hu, "Photoacoustic Tomography: In Vivo Imaging from Organelles to Organs," *Science*, **335**, pp. 1458-1462, 2012.

[2] M. Xu and L. V. Wang, "Photoacoustic imaging in biomedicine," *Rev. Sci. Instrum.*, **77**, pp. 041101-1-22, 2006.

[3] B. E. Treeby, E. Z. Zhang and B. T. Cox, "Photoacoustic tomography in absorbing acoustic media using time reversal," *Inverse Probl.*, **26**, pp. 115003-115023, 2010.

[4] J. Laufer, B. Cox, E. Zang and P. Beard, "Quantitative determination of chromophore concentrations from 2D photoacoustic images using a nonlinear model-based inversion scheme," *Appl. Opt.*, **49**, pp.1219-1233, 2010.

[5] Z. Yuan, Q. Wang and H. Jiang, "Reconstrcution of optical absorption coefficient map of heterogeneous media by photoacoustic tomography coupled with diffusion equation based regularized Newton method," *Opt. Express*, **15**, pp.18076-18081, 2007.

[6] S. Okawa, Y. Hoshi and Y. Yamada, "Improvement of image quality of time-domain diffuse optical tomography with l_p sparsity regularization," *Biomed. Opt. Express*, **2**(12), pp. 3334-3348, 2011.

[7] B. Cox, J. G. Laufer, S. R. Arridge and P. C. Beard "Quantitave spectroscopic photoacoustic imaging: a review," *J. Biomed. Opt.*, **17**, pp. 061202-1-22, 2012.

[8] S. R. Arridge, "Optical tomography in medical imaging," *Inverse Probl.*, **15**, pp. R41-R93, 1999.

[9] C. R. Vogel, Computational Methods for Inverse Problems, The Society of Industrical and Applied Mathematics, 2002.

Improvement in quantifying optical absorption coefficients based on continuous wavelet-transform by correcting distortions in temporal photoacoustic waveforms

Takeshi Hirasawa*[a], Masanori Fujita[b], Shinpei Okawa[a], Toshihiro Kushibiki[a], Miya Ishihara[a]
[a] Dept. of Medical Engineering, National Defense Medical College, 3-2 Namiki, Tokorozawa, Saitama, Japan 359-8513; [b] Div. of Environmental Medicine, National Defense Medical College Research Institute, 3-2 Namiki, Tokorozawa, Saitama, Japan 359-8513;

ABSTRACT

Quantification of the optical absorption coefficients of optical absorbers using photoacoustic (PA) pressure waves with broadband frequency was reported. We proposed to use continuous wavelet-transform (CWT) to obtain time-resolved frequency spectra of PA signals and demonstrated the relationship between optical absorption coefficients of optical absorbers and CWT of PA signals. However, the optical absorption coefficients of the optical absorbers were not quantified. Thus, in this research, we quantified optical absorption coefficients of optical absorbers by using the calibration curve which relates the optical absorption coefficients of optical absorbers and CWTs of PA signals. The calibration curve is derived from the simulation. However, due to the frequency response of the acoustic sensor, the simulated PA pressure waves differed from the measured PA signals. Thus, we measured the frequency response of the acoustic sensor. By convolving the frequency response of the acoustic sensor to the simulated pressure waves, we simulated the PA signals which were obtained by measuring the PA pressure wave using the acoustic sensor. The calibration curve derived from the simulated PA signal enabled to quantify optical absorption coefficients of optical absorbers. We verified the method by quantifying optical absorption coefficients of blood vessel phantoms which is tubes filled with diluted inks with optical absorption coefficients from 10 to 40 cm^{-1}. As results, the simulated PA signals demonstrated close similarity with the measured PA signals, and the optical absorption coefficients of the blood vessel phantoms were quantified with root mean square error of 2.42 cm^{-1}.

Keywords: Continuous wavelet transform, P(VDF-TrFE), optical absorption coefficient, quantification, frequency response, impulse response

1. INTRODUCTION

Photoacoustic (PA) imaging (PAI) is a technique combining ultrasound and optical imaging, which provides tomographic images of optical absorbers in the biological tissues. PA pressure waves which are ultrasounds produced by absorption of pulsed laser lights at optical absorbers are detected by acoustic sensors to form tomographic images. The signals measured by the acoustic sensors are called PA signals. Since the PA pressure waves are produced at the optical absorbers, PAI has a contrast of optical absorption. Since oxy-hemoglobin and deoxy-hemoglobin are dominant endogenous optical absorbers at near-infrared (NIR) wavelength range from 700 to 900 nm, PAI using NIR lights can image these optical absorbers with high sensitively. Furthermore, since oxy-hemoglobin and deoxy-hemoglobin have different absorption spectra in the NIR wavelength range, these optical absorbers can be distinguished from the PA images acquired at multiple wavelengths. By quantifying the optical absorption coefficients at the wavelengths, the concentrations of oxy-hemoglobin and deoxy-hemoglobin can be determined, and then, blood oxygen saturation can be calculated from the concentrations of oxy-hemoglobin and deoxy-hemoglobin. Thus, considerable attentions have been paid to the method to quantify the optical absorption coefficients. The methods determine the absolute value of optical absorption coefficients from the PA signals.

The amplitudes of PA signals have been used to quantify optical absorption coefficients of optical absorbers. Amplitudes of PA signals are proportional to amount of optical energies absorbed by optical absorbers. The amounts of optical energies absorbed by the optical absorbers can be calculated as products of the optical absorption coefficients of the optical absorbers and the optical energy densities (fluence) at the surface of the optical absorbers. Thus, in order to

* Takeshi Hirasawa : E-mail : hirasawa@ndmc.ac.jp, Telephone : +81 4 2995 1596

Photons Plus Ultrasound: Imaging and Sensing 2013, edited by Alexander A. Oraevsky, Lihong V. Wang,
Proc. of SPIE Vol. 8581, 85814J · © 2013 SPIE · CCC code: 1605-7422/13/$18 · doi: 10.1117/12.2006305

obtain the optical absorption coefficient of the optical absorbers, the amplitude of the PA signals should be divided by the fluences at the surface of the optical absorbers. However, the fluences at the surface of the optical absorbers are unknown due to light transport in the biological tissues with strong scattering. This is the essential difficulty with the quantification of the optical absorption coefficients of the optical absorbers from the amplitude of the PA signals. One of the methods to quantify the fluence at the surface of the optical absorber models the light transport with the optical diffusion equation. By solving both of the optical diffusion equation and the acoustic wave equation, the optical absorption coefficient can be quantified [1]. However, since the method has problems of uniqueness and ill-posedness, the calculation method has still being optimized [1, 2].

The temporal waveform can be also used to quantify the optical absorption coefficient of the optical absorber. The temporal waveform of the PA signal reflects the depth profile of the fluence along the acoustic detection axis. Since optical energies absorbed by an optical absorber exponentially attenuate along the light transfer axis, the temporal waveform of the PA signal which is detected in same axis with the light transport reflects exponential attenuation of the fluence. We have been proposing a method to quantify the optical absorption coefficients from temporal waveform of PA signals. In this method, the time-resolved acoustic spectra are calculated from the temporal waveform of PA signal by using continuous-wavelet transform (CWT) [3]. Since this method quantifies the optical absorption coefficient from relative temporal attenuation profiles of the PA signal, the quantified value is independent from the fluence at the surface of the optical absorber. Thus, this method does not require quantifying the fluence at the surfaces of the optical absorbers. We previously reported the relationship between optical absorption coefficients of optical absorbers and the CWT of PA signals [3]. However, the optical absorption coefficients of the optical absorbers have not been quantified. In order to quantify the optical absorption coefficient of the optical absorber, the relationship should be determined by the theoretical analysis. We theoretically analyzed the relationship by the simulation which calculates the PA signal produced from optical absorber with various optical absorption coefficients. Then, we derived the calibration curve which relates the CWT of PA signals to the optical absorption coefficients of optical absorbers from the simulated PA signals. The calibration curve was used to quantify the optical absorption coefficient of the optical absorber from the measured PA signal.

In this paper, we first measured of the frequency responses of the acoustic sensor. We then simulated the PA signal using the frequency response of the acoustic sensor to derive the calibration curve. Finally, the optical absorption coefficients of the blood vessel phantom were quantified from the PA signals.

2. THEORETICAL BACKGROUND

2.1 Detection of PA signal

PA pressure waves were generated by absorption of short pulses of laser lights in optical absorbers. Under the conditions of that the pulse widths of the laser lights are much shorter than the thermal diffusion time in the optical absorbers, the PA pressure waves $p(\mathbf{r}',t)$ can be expressed as following equation, which is derived from the general solution of the PA wave equation in spherical coordinate [4-7] :

$$p(\mathbf{r}',t)=\frac{\beta}{4\pi C_p}\left(\frac{1}{t}\iint_{|\mathbf{r}-\mathbf{r}'|=ct}A(\mathbf{r}-\mathbf{r}')dS\right)*\eta'(t), \qquad (1)$$

where , $\mathbf{r}'$ is the observation point, C_p is the specific heat, β is the isobaric volume expansion coefficient, c is the sound speed, $A(\mathbf{r})$ is the amount of optical energy absorbed at location $\mathbf{r}$, and $\eta'(t)$ is the first derivative of temporal profile of the excitation laser pulse. The PA signal $s(\mathbf{r}',t)$ detected by an acoustic sensor with an impulse response of $m(t)$ is expressed as following [7]

$$s(\mathbf{r}',t)=\frac{\beta}{4\pi C_p}\left(\frac{1}{t}\iint_{|\mathbf{r}-\mathbf{r}'|=ct}A(\mathbf{r}-\mathbf{r}')dS\right)*\eta'(t)*m(t) \quad . \qquad (2)$$

3. MEASUREMENT OF FREQUENCY RESPONSE OF ACOUSTIC SENSOR

3.1 Impulse response method

One of a standard method to measure a frequency response of an acoustic sensor is the secondary calibration method [7, 8], in which a wide-band acoustic pulse is created, and then measured by both of a pre-calibrated hydrophone and the acoustic sensor to be calibrated. However, the method offers only the amplitude data of the frequency response, because the phase data of the frequency response of the reference hydrophone has not been commercially available [9]. The phased data is necessary to obtain a PA pressure wave from a PA signal detected by the acoustic sensor. In order to obtain the phased data of the frequency response, we used impulse response method to calibrate the acoustic sensor, in which the frequency response of the acoustic sensor was calculated from a PA signal produced from a focal point of the laser light [7].

If the laser pulse was absorbed at the focal point of laser light $\mathbf{r}_f$, the absorbed optical energy $A(\mathbf{r}-\mathbf{r}')$ in equation (1) and (2) can be replaced to the Dirac-delta function $\delta(\mathbf{r}_f-\mathbf{r}')$, then, the equation (2) can be rewritten as

$$\begin{aligned} s(\mathbf{r}',t) &= \frac{\beta}{4\pi C_p}\left(\frac{1}{t}\iint_{|\mathbf{r}-\mathbf{r}'|=ct}\delta(\mathbf{r}_f-\mathbf{r}')dS\right)*\eta'(t)*m(t) \\ &= \frac{\beta}{4\pi C_p}\frac{c}{|\mathbf{r}_f-\mathbf{r}'|}\eta'\left(t-\frac{|\mathbf{r}_f-\mathbf{r}'|}{c}\right)*m(t) \end{aligned} \qquad (3)$$

Equation (3) clearly shows that the temporal waveform of the PA signal depends on only the temporal profile of the laser pulse and the impulse response of the acoustic sensor [5, 7]. The frequency spectrum of the PA signal $S(\mathbf{r}',f)$ can be expressed as

$$S(\mathbf{r}',f) = \frac{\beta}{4\pi C_p}\frac{c}{|\mathbf{r}_f-\mathbf{r}'|}\cdot j\cdot 2\pi\cdot f\cdot \mathrm{I}(f)\cdot\exp\left\{-j\cdot 2\pi\cdot f\cdot\frac{|\mathbf{r}_f-\mathbf{r}'|}{c}\right\}\cdot M(f), \qquad (4)$$

$$M(f) = -j\cdot A\cdot\exp\left\{j\cdot 2\pi\cdot f\cdot\frac{|\mathbf{r}_f-\mathbf{r}'|}{c}\right\}\cdot\frac{S(\mathbf{r}',f)}{f\cdot \mathrm{I}(f)}, \qquad (5)$$

where, A is frequency independent constant, $I(f)$ is Fourier transform of the temporal profile of the laser pulse, and $M(f)$ is the frequency response of the acoustic sensor, which is the Fourier transform of the impulse response.

3.2 Experimental setup to measure the frequency response

The PA pressure wave was produced at a surface of a thick black silicone sheet with high optical absorption coefficient. The laser pulses produced from a tunable Ti:sapphire laser (LT-2211, Lotis Tii, Minsk, Belarus) pumped by the second harmonic of a Q-switched Nd:YAG laser (LS-2134, Lotis Tii, Minsk, Belarus) with pulse width of 20 ns, and wavelength of 720 nm were focused by a convex lens with a focal length of 300 mm, and then irradiated to the surface of the black silicone sheet to produce the PA pressure wave. The PA pressure wave was measured by the specially designed ring-shaped acoustic sensor to be calibrated. The detection element of the acoustic sensor was made of a piezoelectric film P(VDF-TrFE) (KF piezo-film, Kureha corp., Tokyo, Japan) which has frequency bandwidth wider than that of a piezoelectric ceramic PZT. The inner and outer diameters of the acoustic sensor were 0.7 mm and 3.0 mm, respectively. The acoustic sensor was placed 45 mm away from surface of the black silicone sheet. Both of the acoustic sensor and the black silicone sheet were immersed in degassed water. The distance was approximately 54 times larger than the near field distance. The PA signal detected the acoustic sensor was amplified by a FET amplifier (SA-220F5, NF Electronic Instruments, Yokohama), and then recorded by a digital oscilloscope (DSO8104A, Agilent technology, Santa Clara, CA, USA) with a sampling rate of 2 GSa/s.

4. QUANTIFICATION OF OPTICAL ABSORPTION COEFFICIENT

4.1 Experimental setup

We used the reflection-mode PA measurement system in which, the irradiation of laser pulse and the detection of PA signal were from the same side of the sample. The pulsed lights described in previous section were coupled into a multi-mode optical fiber with a core diameter of 400 um (M40L02, Thorlabs, Newton, NJ, USA). The other end of the optical fiber was attached to a center of a specially designed ring-shaped acoustic sensor described in previous section.

We performed the experiment using tube phantoms which emulates blood vessels to demonstrate the feasibility to determine the optical absorption coefficient of the optical absorber. Tube phantoms were filled with the black ink (Black Ink, Pilot, Tokyo, Japan) diluted with water in 6 concentrations. Optical absorption coefficients of diluted inks were measured by using spectrophotometer (U-3300, Hitachi High-technologies, Tokyo, Japan). The optical scattering coefficient of the ink assumed negligibly small. The optical absorption coefficients of the diluted inks at the wavelength of 720 nm were 13, 17, 22, 26, 30, and 35 cm^{-1}, respectively. The tubes (Extension tube X2, Top corp., Tokyo, Japan) made of polyvinyl chloride (PVC) had inner and outer diameters of 2.2 mm and 3.5 mm, respectively. The tube was fixed in a direction perpendicular to the detection axis of the acoustic sensor. Distance between the tube and the acoustic sensor was 45 mm. Both of the tube and the acoustic sensor were immersed in degassed water.

4.2 Numerical simulation of PA signal

In order to derive the calibration curve, we calculated the PA pressure wave produced from a tube filled with optical absorbers using equation (1). The amount of optical energy absorbed by the optical absorbers with optical absorption coefficient of μ_a was calculated by using following equations in spherical coordinate

$$A(r,\theta,\varphi)=\frac{F_0}{2\pi(1-\cos\theta_{fiber})\cdot r^2}\cdot\mu_a(r,\theta,\varphi)\cdot\exp\left(-\int_0^r\mu_a(r',\theta,\varphi)dr'\right), \quad (6)$$

$$\mu_a(r,\theta,\varphi)=\mu_a \quad \left(\frac{r}{\cos\theta}-z_0\right)^2+\left(\frac{r}{\sin\theta\cos\varphi}\right)^2<a \quad , \quad (7)$$

where, F_0 is the fluence at the output end of the optical fiber, θ_{fiber} is the divergence angle of the laser light delivered through the optical fiber, a is the inner radius of the tube, and z_0 is distance between the optical fiber and the tube.

In order to simulate the PA pressure wave arrive at the surface of the ring shaped acoustic sensor, the ring shaped detection surface of the acoustic sensor was discretized into small elements. The PA pressure wave arrive at each element were calculated from equation (1). Then, numerical integral was performed to simulate the total PA pressure wave arrive at the acoustic sensor [10].

4.3 Continuous wavelet transform of PA signal using complex Morlet wavelet

The CWT is a time-resolved spectral analysis method which offers time-resolved frequency spectra of PA signals [11-13]. The CWT of a signal $T(a,b)$ is defined as the convolution of the temporal signal $p(t)$ and the wavelet function $\Psi(t)$:

$$T(a,b)=a^{-\frac{1}{2}}\int_{-\infty}^{\infty}p(t)\cdot\Psi^*\left(\frac{t-b}{a}\right)dt, \quad (8)$$

where $\Psi(t)^*$ is the complex conjugate of $\Psi(t)$, a is the dilation parameter and b is the location parameter. We used the complex Morlet wavelet expressed as following equation [11]:

$$\Psi(t)=\pi^{-\frac{1}{4}}\left(e^{-i\omega_0 t}-e^{-\omega_0^2 t}\right)\cdot e^{-\frac{t^2}{2}}, \quad (9)$$

where, ω_0 is the central frequency of the wavelet. The dilation parameter a can be converted to the frequency using the equation $f=\omega_0/a$, and the location parameter b equals to the time. Thus, the CWT $T(a,b)$ can be express as a function of time and frequency $T(f,t)=T(\omega_0/a,b)$.

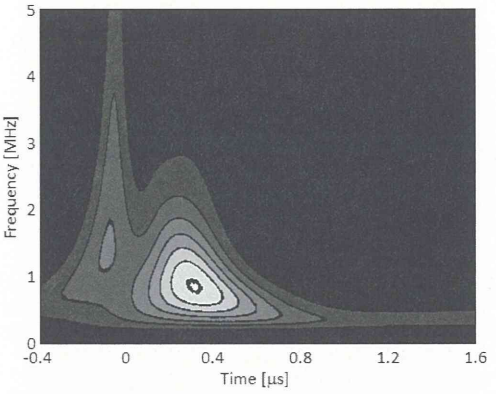

Fig. 1 (a) The contour plot of the CWT. The CWT was calculated from the PA signal produced from the tube filled with a diluted ink with an optical absorption coefficient of 30 cm^{-1}.

The CWT of the PA signal produced from the tube filled with a diluted ink with an optical absorption coefficient of 30 cm^{-1}, detected by the acoustic sensor was calculated by using equations (8) and (9). The contour plot of the CWT was shown in Fig. 1(a). The vertical and horizontal axes of the plot are the frequency and the time, respectively. The peak of the temporal waveform of the PA signal was observed at time 0 μs. The vertical profiles of the plot relate to the frequency spectra at each time. The peaks of the frequency spectra are the instantaneous frequency at each time. The instantaneous frequencies calculated from CWT are shown in Fig. 1(b). The instantaneous frequency has two peaks at times -0.1 μs and 0.3 μs, respectively. We had reported that the first peak of the instantaneous frequency at the first peak of CWT reflects the optical absorption coefficient [3]. Thus, we used the first peak of the instantaneous frequency as a parameter to quantify the optical absorption coefficient.

4.4 Results of experiments and numerical simulations

The relationship between optical absorption coefficients of optical absorbers and the first peaks of the instantaneous frequencies calculated from both of the measured PA signals (square, blue) are shown in Fig. 2(a). The first peaks of instantaneous frequencies calculated from the simulated PA signals are also shown in Fig. 2(a) (circle, red). The simulated PA signal was obtained by convolving the frequency response of the acoustic sensor to the simulated PA pressure wave. The frequency response was measured by the impulse response method. The first peaks of instantaneous frequencies of the simulated PA signals demonstrated close similarities with that of the measured PA signals.

The optical absorption coefficients of the optical absorbers were quantified by comparing the simulated PA signals and the measured PA signals. We derived calibration curve which relates the first peak of instantaneous frequency to the optical absorption coefficient from the simulated PA signals. The calibration curve is also shown in Fig.2(a). By using the calibration curve, the optical absorption coefficients were quantified from the first peaks of instantaneous frequencies. The optical absorption coefficients of the optical absorbers quantified by using this method are shown in Fig. 2(b). The obtained results were found to be in close agreement with the spectrophotometer measurements. In order to verify the accuracy of quantified value, root mean square errors (RMSE) was calculated using following equation :

$$RMSE = \sqrt{\frac{1}{N}\sum_{i=1}^{N}\left(PA\mu_a - spectrophotometer\mu_a\right)^2} \quad . \qquad (10)$$

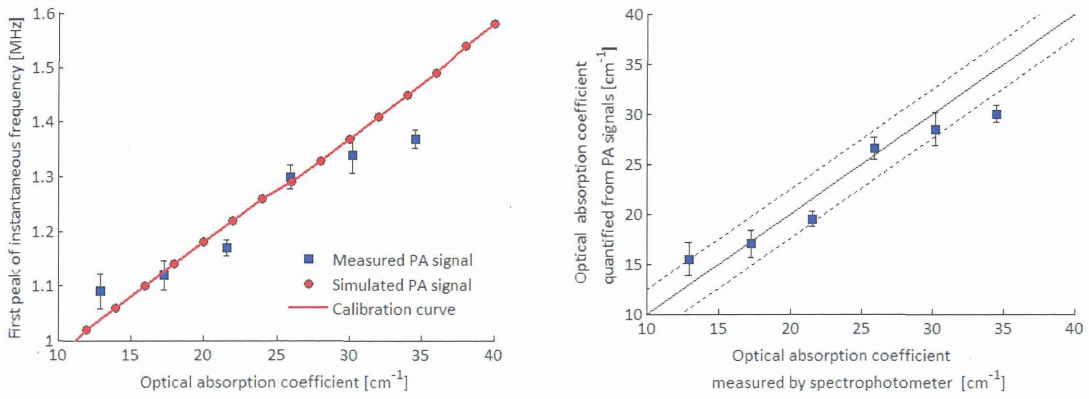

(a) (b)

Fig. 2 (a) Relationship between optical absorption coefficients of optical absorber in the tube and the first peaks of the instantaneous frequencies. The first peak of instantaneous frequencies were calculated from measured PA signal (square, blue) and simulated PA signal (circle, red). The calibration curve (solid line, red) which relates the first peak of instantaneous frequency and the optical absorption coefficient was obtained from simulated PA signal. (b) The optical absorption coefficients determined from the PA signals compared to the spectrophotometer measurements for each optical absorbers in the tube. The solid line is the line of unity and the dotted lines indicates error of 2.42 cm^{-1}. (Error bars : standard deviation, N=4).

The RMSE in optical absorption coefficient was 2.42 cm^{-1}. Errors shown in the value calculated from the PA signals were mainly caused by the mismatch of the experimental condition and the simulation model due to the uncertainty of the experimental setup. In order to reduce the errors, robustness for the mismatch should be improved. Other problems of this method are the effect of the shape of optical absorber. Not only the optical absorption coefficients, but also the shapes of the optical absorbers affect the frequency contents of the PA pressure waves. By focusing the sensitive area of the acoustic sensor, the effect of the shape of the optical absorbers can be reduced. Currently, we are developing the acoustic sensor with focused sensitive area to reduce the effect of the shape.

5. CONCLUSION

We have proposed a method to quantify optical absorption coefficients of optical absorbers from PA signals using CWT. In this method, the first peak of instantaneous frequency was calculated from the CWT of the PA signal as a parameter to quantify the optical absorption coefficient of the optical absorbers. The first peak of instantaneous frequency was converted to the optical absorption coefficient using the calibration line. The calibration line was obtained from the simulated PA signal. The simulated PA signal was obtained by convolving the frequency response of the acoustic sensor to the simulated PA pressure wave.

In order to verify the proposed method, we quantified the optical absorption coefficients of the blood vessel phantom which is made of tubes filled with diluted inks with optical absorption coefficients from 10 to 40 cm^{-1}. As results, the simulated PA signals demonstrated close similarity with the measured PA signals, and the optical absorption coefficients of the phantoms were quantified with root mean square error of 2.42 cm^{-1}.

6. ACKNOWLEDGEMENT

This research was partially supported by Health and Labor Science Research Grant for Research on Medical Device Development, and JST Collaborative Research Based on Industrial Demand (In vivo Molecular Imaging : Towards Biophotonics Innovations in Medicine). Authors appreciate the contribution for this study with Ms. M. Tanikawa and Ms. Y. Mayumi. Experiments were supported by Laboratory Center, National Defense Medical College and Center for Laboratory Animal Experiment, National Defense Medical College.

REFERENCE LINKING

[1] J. Laufer, B. Cox, E. Zhang *et al.*, "Quantitative determination of chromophore concentrations from 2D photoacoustic images using a nonlinear model-based inversion scheme," Appl Opt, 49(8), 1219-1233 (2010).

[2] B. Cox, J. G. Laufer, S. R. Arridge *et al.*, "Quantitative spectroscopic photoacoustic imaging: a review," J Biomed Opt, 17(6), 061202 (2012).

[3] T. Hirasawa, M. Ishihara, K. Tsujita *et al.*, "Continuous wavelet-transform analysis of photoacoustic signal waveform to determine optical absorption coefficient," Proc. SPIE. 8223, 822333 (2012).

[4] K. Irisawa, T. Hirasawa, K. Hirota *et al.*, "Influence of laser pulse width to the photoacoustic temporal waveform and the image resolution with a solid state excitation laser," Proc. SPIE. 8223, 82232W (2012).

[5] Y. Wang, and R. Wang, "Photoacoustic recovery of an absolute optical absorption coefficient with an exact solution of a wave equation," Phys Med Biol, 53(21), 6167-77 (2008).

[6] C. Li, and L. V. Wang, "Photoacoustic tomography and sensing in biomedicine," Phys Med Biol, 54(19), R59-97 (2009).

[7] A. Rosenthal, V. Ntziachristos, and D. Razansky, "Optoacoustic methods for frequency calibration of ultrasonic sensors," IEEE Trans Ultrason Ferroelectr Freq Control, 58(2), 316-26 (2011).

[8] V. Wilkens, and C. Koch, "Amplitude and phase calibration of hydrophones up to 70 MHz using broadband pulse excitation and an optical reference hydrophone," The Journal of the Acoustical Society of America, 115, 2892 (2004).

[9] A. Hurrell, "Voltage to pressure conversion: are you gettingphased'by the problem?," Journal of Physics: Conference Series. 1, 57 (2004).

[10] J. Gamelin, A. Aguirre, A. Maurudis *et al.*, "Curved array photoacoustic tomographic system for small animal imaging," J Biomed Opt, 13(2), 024007 (2008).

[11] P. Addison, J. Watson, and T. FENG, "Low-oscillation complex wavelets," Journal of Sound and Vibration, 254(4), 733-762 (2002).

[12] J. A. Viator, B. Choi, M. Ambrose *et al.*, "In vivo Port-Wine Stain Depth Determination with a Photoacoustic Probe," Appl Opt, 42(16), 3215-3224 (2003).

[13] S. H. Holan, and J. A. Viator, "Automated wavelet denoising of photoacoustic signals for circulating melanoma cell detection and burn image reconstruction," Phys Med Biol, 53, N227 (2008).

O3-08-8

Optical absorption coefficient determination from photoacoustic waveform using continuous wavelet transform

Takeshi Hirasawa[1], Toshihiro Kushibiki[1], Masanori Fujita[2], Miya Ishihara[1]
[1]Department of Medical Engineering, National Defense Medical College
[2]Division of Environmental Medicine, National Defense Medical College Research Institute

Abstract: In photo-acoustic (PA) imaging, valuable medical applications based on the optical absorption spectrum such as blood oxygenation imaging have been investigated. Accurate determination of optical absorption coefficients is essential for these applications. Although amplitudes of PA signals have been commonly used to determine optical absorption coefficients of optical absorbers in biological tissues, amplitudes of PA signals are decreased by optical attenuation in surrounding tissues. We propose a method for determining optical absorption coefficients from temporal waveforms of PA signals using continuous wavelet transform (CWT). Temporal waveforms of PA signals are associated with spatial profiles rather than amplitudes of absorbed optical energies. Thus, this method not greatly affected by optical attenuation in surrounding tissue. Peak frequencies of the time resolved frequency spectra calculated by using CWT was used to determine optical absorption coefficients. As a result of experiment using phantoms, correlations of the peak frequencies of CWT with optical absorption coefficients of the phantoms were confirmed.
Keywords: optical property, oxygen saturation, molecular imaging, frequency spectrum, P(VDF-TrFE)

1. Introduction

Optical absorption coefficients of biological tissues are closely associated with physiological parameters such as concentrations and oxygenation of hemoglobin [1-4]. Several optical imaging techniques such as diffuse optical tomography have been developed to measure optical absorption coefficients. However, spatial resolutions of these techniques have been limited by strong optical scattering of biological tissues.

Photo-acoustic (PA) imaging (PAI) is an imaging technique combining ultrasound and optical imaging [1]. In this technique, optical absorbers in biological tissues such as hemoglobin are illuminated by a nanosecond pulse laser to produce broadband ultrasound (PA signal) then, PA signals are detected by ultrasound sensors. Since ultrasound scattering is much weaker than optical scattering in biological tissues, PAI is capable of high resolution imaging (~1mm) at depths beyond limitations of optical imaging techniques due to optical scattering. The amplitude of the PA signal is directly proportional to the absorbed optical energy which in turn is a function of optical absorption coefficients of biological tissues. By varying the wavelength of excitation pulses, spectroscopic information can be obtained. The multispectral PA imaging acquires the spatial distribution of optical absorption spectra to quantify concentrations of chromophore. By quantifying concentrations of oxy hemoglobin and deoxy hemoglobin, the oxygen saturation of hemoglobin can be calculated.

PA images are spatial mapping of the absorbed optical energy E(mJ cm^{-3}), which is the product of the optical absorption coefficient μ_a(cm^{-1}) and the fluence F (mJ cm^{-2}) [2]. The fluence at a surface of the optical absorber in biological tissues is attenuated by surrounding tissues and varies with wavelength due to spectral dependence of optical properties of surrounding tissues [3]. Thus, in order to quantify the μ_a of the biological tissue, compensation of the fluence attenuation has been required. Currently, effects of the fluence attenuation have been compensated by solving the coupled radiation transfer equation and PA wave equation [4]. However, the calculation requires some assumptions to obtain a unique solution and it is time-consuming. These factors have limited the applicability of this method.

We propose a method for determining the μ_a using a temporal waveform of the PA signal. This method is not greatly affected by optical attenuation in surrounding tissue, because the temporal waveform of the PA signal depends on the spatial profile of absorbed optical energy along the detection axis of the ultrasound sensor rather than the amplitude of absorbed optical energy. Thus, the μ_a can be determined without a compensation of the fluence attenuation. However, the temporal waveform of the PA signal is strongly affected by noise due to the low signal-to-noise ratio (SNR). We focused onto the frequency spectrum of PA signals to reduce effects of noise. Continuous wavelet transform (CWT) which is a time-resolved frequency spectrum analysis was used to obtain frequency spectrum maintaining the temporal resolution. We report the result of CWT for the PA signals from several phantoms with various μ_a.

2. Materials and methods

2-1. PA signal analysis using CWT

Continuous wavelet transform is a time resolved frequency spectrum analysis method. Since the PA signal is a pulse wave generated by irradiation of a laser pulse, sensitivity for temporal changes of the frequency spectrum was required for an analysis method. Thus we adopted CWT as the analysis method which has scalable temporal resolution and frequency resolution. The detailed description of CWT was shown in references [5, 6]. In this research, we chose the complex-morlet wavelet that is the product of a complex sinusoidal function and a Gaussian function as the mother wavelet of CWT. The CWT of the PA signal is the 2D matrix complex data with the vertical axis is associated with frequency and the horizontal axis is associated with time. In order to improve the temporal resolution of complex-morlet wavelet, the number of sinusoidal waves in a Gaussian function was decreased, and the appropriate offset was added to sinusoidal function [5].

The intensity of CWT is associated with the power spectrum of the PA signal. We extracted the parameter to determine the μ_a by comparing the μ_a and the absolute value of CWT.

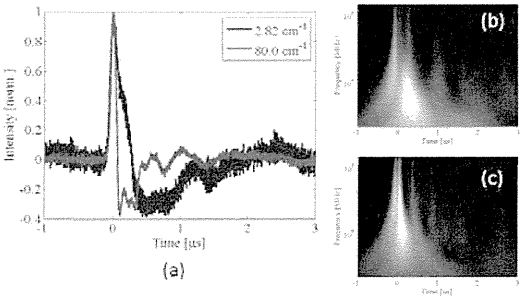

Fig. 1 (a) PA signals generated from phantoms with μ_a of 2.82cm^{-1} and 80.0 cm^{-1}, (b, c) CWTs of PA signals generated from the phantom with μ_a of 2.82cm^{-1} (b) and 80.0 cm^{-1} (c).

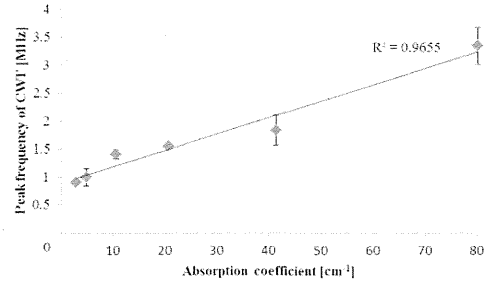

Fig. 2 Relationships of optical absorption coefficients with the peak frequencies of CWT, The error bar expresses standard deviation of measurements (n=4).

2-2. PA signal measurement using phantoms

We measured PA signals generated from phantoms. The phantoms consisted of two layers : the upper layer was a transparent layer, and the lower layer was an absorption layer that generated the PA signal. Each layer contained 1.5 wt% of agar and had a thickness of 9.5mm. The lower layers contained black ink as optical absorbers, and their μ_a were 2.82, 4.81, 10.5, 20.6, 41.3, or 80.0 cm^{-1}.

A tunable Ti:sapphire laser (LT2242, Lotis:Tii) pumped by a second-harmonic generation of Nd:YAG laser (LT2211, Lotis:Tii), providing 15ns pulses at the repetition rate of 15Hz was used as the source of excitation pulses to generate the PA signal. The excitation pulse was irradiated to the phantom via an optical fiber with a core diameter of 0.4 mm, and a numerical aperture of 0.39. The wavelength of the excitation pulse was tuned to 720 nm. The wavelength was in a range of the optical window of biological tissue.

In order to analyze the frequency spectrum of the PA signal, an ultrasound sensor with a wide frequency band was required. We used an originally designed ultrasound sensor made of P(VDF-TrFE) to detect PA signal. The ring-shaped detection element of the sensor had an inner diameter of 0.6mm, and an outer diameter of 4.0mm. By passing the optical fiber through the hole of the ring-shaped element, the optical excitation axis and the ultrasound detection axis were aligned coaxially. The PA signal was measured by bringing the ultrasound sensor into contact with the upper layer of the phantom via optical transparent acoustic coupling gel (UF clear gel, FUKUDA Denshi). The detected PA signal was amplified by low noise FET amplifier (SA-220F5, NF Electronic Instruments) and then recorded by digital oscilloscope (DSO8104A, Agilent).

3. Results and discussions

Temporal waveforms of measured PA signals generated from the absorption layers with μ_a of 2.82 cm^{-1} and 80.0 cm^{-1} placed under the optical transparent layer with μ_s' of 0 cm^{-1} are shown in Fig. 1 (a). In order to compare the temporal waveform of the PA signal, the vertical axis of this figure was normalized. The CWTs of the PA signals were also shown in Fig. 1 (b) and Fig. 1 (c). The vertical axis of the CWT represents frequency of the PA signal. As shown in Fig. 1 (c), the PA signal generated from the frequency component. Thus, we used the peak frequency of the CWT as a parameter to determine the μ_a, which is the frequency with the maximum CWT intensity. The peak frequency of CWT was increased from 0.96 MHz to 3.26 MHz by increasing the μ_a from 2.82cm^{-1} to 80.0cm^{-1}. By analyzing the PA signal generated from other phantoms, correlations of the peak frequency of the CWT with the μ_a, with a correlation coefficient of 0.97 was confirmed. However, by focusing onto the μ_a range of 1-20cm^{-1}, the correlation coefficient was decreased to 0.88. Thus, the accuracy especially at low μ_a should be further improved.

For the biomedical application, the effects of optical scattering should be discussed. The optical scattering in surrounding tissue causes not only optical attenuation but also the spatial expansion of the excitation pulse. The spatial expansion of the excitation pulse decreases the frequency of the PA signal. This effect could be prevented by using a focused ultrasound sensor.

4. Conclusions

We proposed a method to determine the μ_a from the temporal waveform of the PA signal. We used CWT to analyze the frequency spectrum of the PA signal maintaining temporal resolution. The parameters associate to power spectrum of the PA signal was obtained by using complex-morlet wavelet as a mother wavelet of CWT. By comparing the CWT and the μ_a of the phantom, correlation of peak frequency of the CWT with the μ_a was confirmed.

Acknowledgement

This research was partially supported by Health and Labour Science Research Grant for Research on Medical Device Development, and JST Collaborative Research Based on Industrial Demand (In vivo Molecular Imaging : Towards Biophotonics Innovations in Medicine).

Reference

[1] C. Li, et al., Phys. Med. Biol., 54, R59-R97 (2009)
[2] Z. Guo, et al., Opt. Lett., 35(12), 2067-2069 (2010)
[3] M. Sivaramakrishnan, et al., Phys. Med. Biol., 52, 1349-1361 (2007)
[4] J. Laufer, et al., Phys. Med. Biol., 52, 141-168 (2007)
[5] P. S. Addison, [The illustrated wavelet transform handbook introductory theory and applications in science, engineering, medicine and finance], IOP Publishing, England (2002)
[6] T. Hirasawa, et al., Proc. Of SPIE, 8223 (in print)

Continuous wavelet-transform analysis of photo-acoustic signal waveform to determine optical absorption coefficient

T. Hirasawa[a], M. Ishihara[a], K. Tsujita[b], K. Hirota[b], K. Irisawa[b], M. Kitagaki[a], M.Fujita[c], M.Kikuchi[d]
[a] Dept. of Medical Engineering, National Defense Medical College, Japan
[b] Medical Systems Research & Development Center, Research & Development Management Headquarters, FUJIFILM Corporation, Japan
[c] Div. of Environmental Medicine, National Defense Medical College Research Institute, Japan
[d] Vice President and Dean, National Defense Medical College , Japan

ABSTRACT

In photo-acoustic (PA) imaging, valuable medical applications based on optical absorption spectrum such as contrast agent imaging and blood oxygen saturation measurement have been investigated. In these applications, there is an essential requirement to determine optical absorption coefficients accurately. In present, PA signal intensities have been commonly used to determine optical absorption coefficients. This method achieves practical accuracy by combining with radiative transfer analysis. However, time consumption of radiative transfer analysis and effects of signal generation efficiencies were problems of this method. In this research, we propose a new method to determine optical absorption coefficients using continuous wavelet transform (CWT). We used CWT to estimate instantaneous frequencies of PA signals which reflects optical absorption distribution. We validated the effectiveness of CWT in determination of optical absorption coefficients through an experiment. In the experiment, planar shaped samples were illuminated to generate PA signal. The PA signal was measured by our fabricated PA probe in which an optical fiber and a ring shaped P(VDF-TrFE) ultrasound sensor were coaxially aligned. Optical properties of samples were adjusted by changing the concentration of dye solution. Tunable Ti:Sapphire laser (690 – 1000 nm) was used as illumination source. As a result, we confirmed strong correlation between optical absorption coefficients of samples and the instantaneous frequency of PA signal obtained by CWT. Advantages of this method were less interference of light transfer and signal generation efficiency.

Keywords: photoacoustic, wavelet, acoustic frequency spectrum, optical absorption coefficient, P(VDF-TrFE)

1. INTRODUCTION

Photo-acoustic (PA) imaging is a combined technique of ultrasound and optical imaging [1]. This technique provides tomographic image of deep biological tissues beyond the limitation of optical imaging due to strong scattering. Multispectral PA imaging has been widely researched as a functional imaging technique taking advantage of optical absorption contrast [2-4]. This technique generally estimates absorption spectrums of biological tissues from spectral dependence of PA images and valuable medical applications of which such as blood oxygenation imaging [3, 4] and molecular imaging [2] were reported. In these applications, in order to identify optical absorbers and quantify their concentrations, accurate optical absorption coefficient determination methods have been required. A peak intensity of a PA signal has been used as a parameter to determine an optical absorption coefficient from a PA image because an initial pressure of PA wave is directly proportional to optical absorption distribution. Maslov et al. reported quantification of blood oxygenation in blood vessels using this parameter [3]. However, in their *in-vivo* experiment, spectral dependences of PA signals were caused by not only absorption spectrums of bloods in blood vessels but also optical attenuation in surrounding tissues . Then, the accuracy of the blood oxygenation quantification was significantly degraded. In order to compensate effects of optical attenuation, Laufer et al. calculated an optical energy distribution by solving the radiation transfer equation [4]. Compensation of optical attenuations improved the accuracy of the optical absorption coefficient determination. However, the calculation requires some assumption to obtain a unique solution and consumes times. These factors have constrained an applicability of this method.

*hirasawa@ndmc.ac.jp: phone +81 4 2995-1596; fax +81 4 2996-5199; address 3-2, Namiki, Tokorozawa, Saitama, Japan, 359-8513

Photons Plus Ultrasound: Imaging and Sensing 2012, edited by Alexander A. Oraevsky, Lihong V. Wang,
Proc. of SPIE Vol. 8223, 822333 · © 2012 SPIE · CCC code: 1605-7422/12/$18 · doi: 10.1117/12.908088

We proposed an optical absorption coefficient determination method using a temporal waveform of a PA signal. The merit of this method is reduced effect of optical attenuation. A temporal waveform of a PA signal also depends on an optical absorption coefficient because an initial pressure of a PA wave is related to an optical absorption distribution. An optical absorption distribution could be expressed as a product of an optical absorption coefficient and an energy distribution. For an optical absorber with uniform optical absorption coefficient, the optical absorption distribution is proportional to the energy distribution which attenuates exponentially with a rate of the optical absorption coefficient. The proposed method does not require absolute PA signal intensity then it is not affected by optical attenuation in surrounding tissue. However, the temporal waveform of the PA signal is strongly affected by noises due to low signal to noise ratio (SNR) of the PA signal.

In this research, in order to reduce effects of noises we focused onto frequency spectrums of PA signals. A frequency spectrum of a PA signal also reflects an optical absorption coefficient and if a principle component of an additive noise in the PA signal is a white noise, the frequency spectrum provides higher SNR than the temporal waveform because the white noise is averaged in the frequency domain. In order to obtain the time resolved frequency spectrum of the PA signal, we introduced continuous wavelet transform (CWT) [6]. One of the features of CWT is a scalable width of time window which enables both high frequency resolution in low frequency component and high temporal resolution in high frequency component.

Some groups already introduced wavelet transform to a PA signal analysis. For examples of noise reduction, J. A. Viator et al. and some groups applied discrete wavelet transform to reduce a white noise from a PA signal [7, 8]. And for an example of a waveform characterization, I. Patrikeev et al. reported correlation between CWT of a simulated PA signal and both concentration and oxygen saturation of hemoglobin [9]. However, the relationship between CWT of PA signals and optical absorption coefficients has not been reported.

We report systematical relationship between optical absorption coefficients and CWT of PA signals. In out experiment, PA signals were generated from several phantoms with different optical absorption coefficients and then measured by P(VDF-TrFE) ultrasound sensor with wide frequency band width.

2. MATERIALS AND METHOD

2.1 Principle

2.1.1 Photo-acoustic signal equation

In condition satisfying acoustically homogeneous and thermal confinement, an acoustic pressure $p(r,t)$ referred as a PA signal is expressed as a follow wave equation.

$$c^2\nabla^2 p(\boldsymbol{r},t) - \frac{\partial^2 p(\boldsymbol{r},t)}{\partial t^2} = -\frac{c^2\beta}{C_p}\frac{\partial H(\boldsymbol{r},t)}{\partial t} \qquad (1)$$

Where, c is a sound speed in medium, C_p is a specific heat at constant pressure, and β is a thermal expansion coefficient, respectively. A heat generation $H(r,t)$ caused by an absorption of excitation laser pulse is expressed as a follow equation.

$$H(\boldsymbol{r},t) = \mu_a(\boldsymbol{r}) \cdot F_o(\boldsymbol{r}) \cdot \eta(t) \qquad (2)$$

Where, $F_o(\boldsymbol{r},t)$ is a local fluence, $\eta(t)$ is a temporal waveform of an excitation laser pulse, and $\mu_a(\boldsymbol{r})$ is an optical absorption coefficient. When the condition of stress confinement is satisfied, $\eta(t)$ can be approximated as the Dirac delta function, and then follow equation can be derived from eq. (1) and eq.(2) using the Green's function expansion [1].

$$p(\boldsymbol{r},t) = \frac{\beta}{4\pi C_p}\frac{\partial}{\partial t}\left[\frac{1}{ct}\int \mu_a(\boldsymbol{r}')F_o(\boldsymbol{r}')\delta\left(t - \frac{|\boldsymbol{r}-\boldsymbol{r}'|}{c}\right)d\boldsymbol{r}'\right] \qquad (3)$$

Where, $\boldsymbol{r}$ is an observation point. We substituted $\boldsymbol{r} = \boldsymbol{0}$ for simplicity and introduced the spherical coordinate then a follow equation was derived.

$$p(\boldsymbol{0},t) = \frac{\beta}{4\pi C_p}\frac{\partial}{\partial t}[ct\iint \mu_a(ct,\theta,\varphi)F_o(ct,\theta,\varphi)sin\theta d\theta d\varphi] \qquad (4)$$

From eq. (4), a temporal waveform of a PA signal corresponds to differential in radial direction of an optical absorption distribution around the observation point. By using Fourier transform, a follow equation is derived.

$$\tilde{p}(\mathbf{0},k) = \frac{\beta}{4\pi C_p} ik \left[\iint \frac{\partial}{\partial k} \{\tilde{\mu}_a(k,\theta,\varphi) * \tilde{F}_o(k,\theta,\varphi)\} sin\theta d\theta d\varphi \right] \quad (5)$$

Where, $\tilde{p}(\mathbf{0},k)$, $\tilde{\mu}_a(k,\theta,\varphi)$, and $\tilde{F}_o(k,\theta,\varphi)$ are Fourier transform of $p(\mathbf{0},t)$, $\mu_a(ct,\theta,\varphi)$, and $F_o(ct,\theta,\varphi)$, respectively. A frequency f can be calculated from a wavenumber k by an equation of $f = ck$. From eq. (5), a frequency spectrum of a PA signal depends on an optical absorption distribution in an optical absorber. In the PA signal acquired using an ultrasound sensor with narrow directionality, integrals in θ, φ axis included in eq. (4) and (5) could be neglected. Further, assuming the optical absorber with homogeneous optical absorption coefficient, the temporal waveform and the frequency spectrum of the PA signal reflects an optical attenuation in the optical absorber which depends on the optical absorption coefficient.

2.1.2 Continuous wavelet transform using Mexican-hat wavelet

Continuous wavelet transform (CWT) is a time resolved frequency spectrum analysis technique. In another time resolved frequency spectrum analysis technique of short time Fourier transform, a constant width of time window results in a lack of a time resolution especially in a high frequency component. On the other hand, a scalable width time window of CWT results both high temporal resolution in high frequency component and high frequency resolution in low frequency component [6].

In CWT, daughter wavelet $\Psi_{a,b}(t)$ is expressed as a follow equation, which is shifted and scaled mother wavelet function $\Psi(t)$ with no DC component and finite time width.

$$\Psi_{a,b}(t) = \frac{1}{\sqrt{a}} \Psi\left(\frac{t-b}{a}\right) \quad (6)$$

Where, a is a scale relates to time domain expansion of wavelet function and b is a shift relates to time domain displacement of wavelet function, respectively. By increasing the scale, the temporal width of the wavelet function is expanded with keeping constant wavenumber then the frequency of the wavelet function is decreased. Conversely, by decreasing the scale, the frequency of the wavelet function is increased. The CWT calculates the wavelet transform $\mathrm{T}(a,b)$ of the PA signal $x(t)$, from a follow convolution integral of the PA signal $x(t)$ and the daughter wavelet $\Psi_{a,b}(t)$.

$$\mathrm{T}(a,b) = \int_{-\infty}^{\infty} x(t)\, \Psi_{a,b}{}^{*}(t) dt \quad (7)$$

Where, $\Psi_{a,b}{}^{*}(t)$ is the complex conjugate of $\Psi_{a,b}(t)$. Since the scale and the shift of the wavelet transform can be converted to a frequency and a time, wavelet transform is equivalent to time resolved frequency spectrum analysis of a signal.

We adopted the Mexican-hat wavelet as the mother wavelet of CWT. This wavelet provides high temporal resolution comparing to other wavelets. This wavelet is second order differential of the Gaussian function which is expressed as follow equation.

$$\Psi(t) = (1-t^2)e^{-\frac{t^2}{2}} \quad (8)$$

The central frequency of this wavelet is $f_0 = \sqrt{2}/2\pi$ and the central frequency of daughter wavelets $\Psi_{a,b}(t)$ could be expressed as $f = f_0/a$. We defined central frequencies of wavelets as pseudo frequencies.

2.2 PA signal measurement using phantom

In order to confirm relationship between CWT of PA signals and optical absorption coefficients of optical absorbers, we measured PA signal using phantoms. The phantoms consisted of two layers, the upper was a turbid layer which simulated optical attenuation due to optical scattering and the lower was an absorption layer which simulated optical absorption in optical absorber and generated PA wave. Both layers contain 1.5 wt% of agar and had thickness of 9.5 mm. Upper layers contain 0, 1.16, 2.33, 4.67 vt% of intralipos (Otsuka Pharmaceutical) as optical scatterers. The 4.67 vt% intralipos had the reduced scattering coefficient of $\mu_s' = 10\mathrm{cm}^{-1}$ which was nearly equal to that of a muscle tissue [10, 11]. Lowers layer contain 1, 2, 4, 8, 16, 32 vt% of black ink (BI) as optical absorbers. The 1 vt% BI had the absorption coefficient of $\mu_a = 2.82\ cm^{-1}$ for the wavelength of 720 nm.

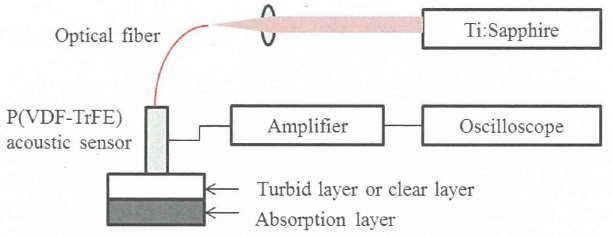

Fig.1 Schematic diagram of an experimental setup

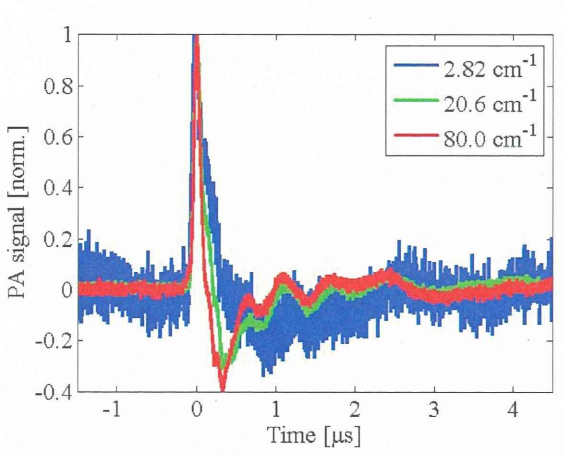

Fig. 2 Temporal waveform of PA signal generated from absorption layer with various concentrations of black ink. Amplitude of PA signal is normalized to have peak intensity of 1. The waveforms were shifted in time domain to have peak intensities at 0 μs.

Schematic diagram of the experimental setup is shown on fig.1. A Tunable Ti:Sapphire laser (LT2242, Lotis:Tii) pumped by second harmonic of Q-switched Nd:YAG laser was used to generate excitation laser pulse. The wavelength of the laser pulse was tuned to 720 nm. This wavelength of light penetrates relatively deeply into biological tissues. The excitation laser pulse with a width of 15ns was irradiated to phantoms via an optical fiber with a core diameter of 400 μm and a numerical aperture of 0.48. In order to prevent saturation of a detection system described below, the pulse energy of the laser pulse was attenuated by ND filters before fiber coupling.

Since frequency spectrums of PA signals expressed as eq.(5) depends on optical absorption coefficients of phantoms and generally has wide frequency band width, an ultrasound sensor with a wide frequency band width is required. Then, we used our originally designed ultrasound sensor made of piezoelectric polymer P(VDF-TrFE) to detect the PA signal. The piezoelectric film P(VDF-TrFE) has relatively wide frequency band width than conventional ultrasound sensors made of piezoelectric ceramic PZT. The ring shaped detection element of the sensor had an inner diameter of 0.6mm and an outer diameter of 4.0 mm respectively. By passing the optical fiber into the hole of the ring shaped element, the optical excitation axis and the ultrasound detection axis were aligned coaxially.

PA signals generated from phantoms were measured by contacting the ultrasound sensor to phantoms surfaces via optical transparent acoustic coupling gel (UF clear gel, FUKUDA-Denshi). The PA signal detected by the ultrasound sensor is amplified by a FET amplifier (SA-220F5, NF Electronic Instruments, 46 dB, 0.1 – 80 MHz) and then, memorized by a digital oscilloscope (DSO8104A, Agilent, 4 GSa/s).

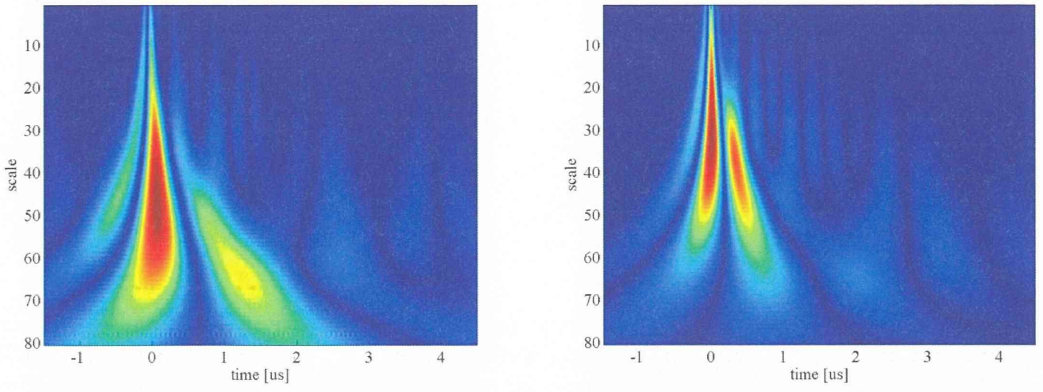

(a) μ_a =2.82 cm^{-1} (b) μ_a =80.0 cm^{-1}

Fig. 3 Scalograms of photo-acoustic signals obtained using Mexican hat wavelet transform.

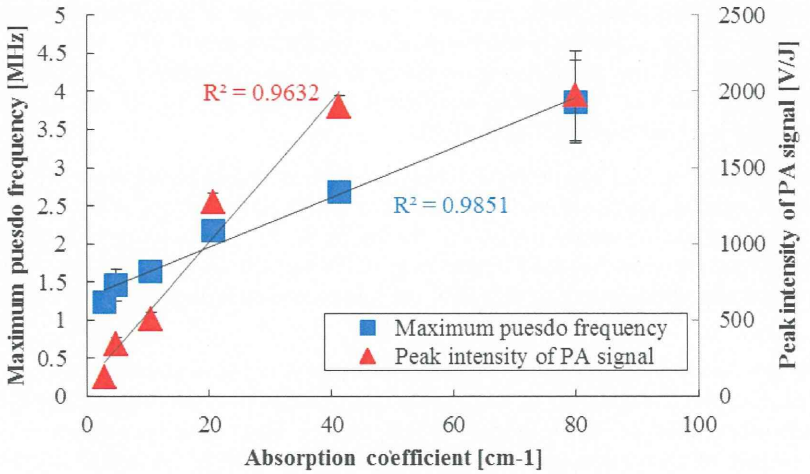

Fig.4 Relationship between optical absorption coefficients and maximum pseudo frequency or PA signals intensity. Maximum pseudo frequency is calculated from wavelet scale with largest wavelet coefficient. The error bar expresses standard deviation of measurements with N=4.

3. RESULTS AND DISCUSSION

Temporal waveforms of PA signals generated from absorption layers with absorption coefficients of 2.82 cm^{-1} and 80.0 cm^{-1} placed under a clear layer is shown on fig.2. In order to compare waveforms of PA signals, voltages of each PA signals were normalized to have maximum intensities of 1. Fig.3 shows results of CWT for PA signals generated from absorption layers with absorption coefficients of 2.82 cm^{-1} and 80.0 cm^{-1}. Images shown on fig.3 were referred as scalograms which expresses intensities of CWT T(a, b). The vertical axis of a scalogram is scale a and the other axis is shift b, and these parameters relate to frequency and time respectively. By comparing scalograms shown on fig.3, the PA signal generated from the phantom with the absorption coefficient of 80.0 cm^{-1} had strong peak at lower scale (high frequency) component. Then we used maximum pseudo frequency as a parameter to determine optical absorption coefficient. Maximum pseudo frequency was converted from the scale value. Fig.4 shows relationship between maximum pseudo frequency and optical absorption coefficient. Maximum intensities of PA signals were also plotted on fig.4, which were commonly used to determine optical absorption coefficient.

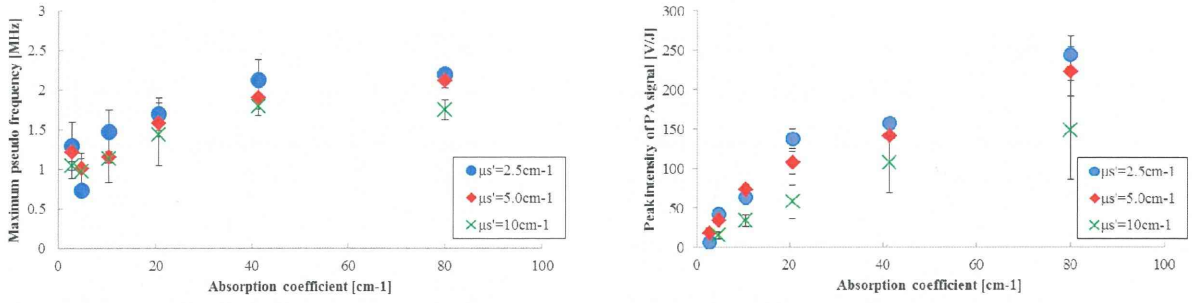

Fig.5 Left: Relationship between Maximum pseudo frequency and absorption coefficient of optical absorber placed under the turbid phantoms with various reduced scattering coefficients. Right: ship between peak intensity of PA signal and absorption coefficient of optical absorber placed under the turbid phantoms with various reduced scattering coefficients. The error bar expresses standard deviation of measurements with N=4.

As shown on fig.4, both peak intensities and maximum pseudo frequencies had linear relationship with optical absorption coefficients. However, at range of optical absorption coefficients greater than 40 cm^{-1}, the increase of peak intensities were saturated. On the other hand, maximum pseudo frequency kept linearity through optical absorption coefficient range measured in this experiment and correlation coefficient was 0.985. Maximum pseudo frequencies at absorption coefficients of 10 – 80 cm^{-1} were dominant factor to increase correlation coefficient then, by focusing onto absorption coefficients of 1 – 10 cm^{-1}, correlation coefficient decreased to 0.887. Then, linearity in lower absorption coefficient range was one of the challenges of this method.

In order to validate effects of optical scattering of biological tissues, turbid layers were placed onto absorption layers and then PA signal was measured. The measured PA signal was analyzed by using CWT. Fig.5 shows maximum pseudo frequencies and PA signal intensities respectively. As shown in fig.5, maximum pseudo frequencies increased with optical absorption coefficients however, pseudo frequencies of PA signals shown in fig.5 were lower than that of fig.3. For example, in case of the absorption coefficient is 80.0 cm^{-1}, the maximum pseudo frequency was decreased from 3.86 MHz to 1.79 MHz.

This effect could be prevented by focusing the sensitive area of the ultrasound sensor because this effect was caused by spatial expansion of the optical absorption area at the surface of absorption layer due to optical diffusion in the turbid layer. The ultrasound sensor used in this experiment had narrow directionality and approximately 4mm diameter sensitive area on the surface of absorption layer. Then, temporal expansion of PA signal could be calculated as 308 ns from the sensitive area of ultrasound sensor and the distance between the ultrasound sensor and the absorption layer. This calculated temporal expansion of the PA signal almost coincided with the decrease of the maximum pseudo frequency. Then, the decrease of maximum pseudo frequency was caused by expansion of optical absorption area on the surface of absorption layer. By focusing the sensitive area of ultrasound sensor, the sensor will not sense the PA signal induced at expanded area then, the effect of optical diffusion could be reduced. However, optical scattering and thickness of samples may suffer optical penetration depth especially for optical absorber with low absorption coefficient then, further discussion is required.

On the other hand, maximum intensities of PA signals were decreased by increasing optical scattering coefficients. In case of the absorption coefficient is 80.0 cm^{-1}, peak intensity decreased 1970.5 V/J to 148.6 V/J due to optical scattering. Then, in order to estimate optical absorption coefficient of absorption layer from maximum intensity of PA signal, optical attenuation should be compensated. So, optical absorption coefficient determination using CWT have potential to be the alternative method.

4. CONCLUSION

We proposed an optical absorption coefficient determination method using CWT which does not require optical energy distribution compensation because it was less affected by optical attenuation. We defined the parameter maximum pseudo frequency to determine optical absorption coefficient. The parameter was calculated from the scale with maximum intensity in CWT of PA the signal. We measured PA signal using phantom in order to confirm the correlation between optical absorption coefficients and maximum pseudo frequencies. As results, maximum pseudo frequencies had linear relationship with optical absorption coefficients through a wider range of absorption coefficients comparing to peak intensity of PA signal. However, by placing optical scatterer between sensor and absorption layer, frequency of PA signal was decreased. This effect was caused by expansion of optical absorption area on the surface of absorption layer and which could be prevented by focusing sensitive area of ultrasound sensor. Then, CWT has potential as an alternative optical absorption coefficient determination method.

5. ACKNOWLEDGEMENTS

This work has been partially supported by Health and Labour Sciences Research Grants for Research on Medical Device Development, and Magnetic Health Science Foundation. Authors appreciate the important contribution for this study with Mr. K. Hirota and Mr. T. Abe(FUJIFILM Corp.). Authors thank Ms. M. Tanikawa and Ms. Y. Mayumi for their contributions for experiment. Experiments were also supported by Laboratory Center, National Defense Medical College and Center for Laboratory Animal Experiment, National Defense Medical College.

REFERENCES

[1] Li, C., and Wang, L. V., "Photoacoustic tomography and sensing in biomedicine", Phys. Med. Biol., 54, R59-R97 (2009)

[2] Zerda, A., Liu, Z., Bodapati, S., Teed, R., Vaithilingam, S., Khuri-Yakub, B. T., Chen, X., Dai., H., and Gamchir, S. S., "Ultrahigh sensitivity carbon nanotube agents for photoacoustic molecular imaging in living mice", Nano Lett., 10, 2168-2172 (2010)

[3] Sivaramakrishnan, M., Maslov, K., Zhang, H. F., Stica, G., and Wang, L. V., "Limitaitons of quantitative photoacousitc measurement of blood oxygenation in small vessels", Phys. Med. Biol., 52, 1349-1361 (2007)

[4] Laufer, J., Delpy, D., Elwell, C., and Beard, P., "Quantitative spatially resolved measurement of tissue chromophore concentrations using photoacoustic spectroscopy : application to the measurement of blood oxygenation and hemoglobin concentration", Phys. Med. Biol., 52, 141-168 (2007)

[5] Ishihara, M., Hirasawa, T., Tsujita, K., Kitagaki, M., Bansaku, I., Fujita, M., and Kikuchi, M., "Multifunctional photoacoustic signals detected by P(VDF-TrFE) film sensor with a wide range of frequency", Proc. of SPIE, 7899, 78992Z-1 - 78992Z-5 (2011)

[6] Addison, P. S., "The illustrated wavelet transform handbook introductory theory and applications in science, engineering, medicine and finance", IOP Publishing, England (2002)

[7] Patrikeev, I., Brecht, H. –P., Petrov, Y. Y., Petrova, I. Y., Prough, D. S., and Esenaliev, R. O., "Wavelet differentiation of optoacoustic signals for monitoring of total hemoglobin concentration and oxygen satulation level in small blood vessels", Proc. of SPIE, 6437, 643717-1 – 643717-6 (2007)

[8] Holan, S. H., and Viator, J. A., "Automated wavelet denoising of photoacoustic signals for circulating melanoma cell detection and burn image reconstruction", Phys. Med. Biol., 53, N227-N236 (2008)

[9] Lu, T., Jiang, J., Su, Y., Song, Z., Yao, J., and Wang, R. K., "Signal processing using wavelet transform in photoacoustic tomography", Proc. of SPIE, 6439, 64390L-1 – 64390L-6 (2007)

[10] Staveren, H. J., Moes, C. J. M., Marle, J., Prahl, S. A., and Gemert, M. J. C., "Light scattering in intralipid-10% in the wavelength range of 400-1100nm", Applied Optics, 30(31), 4507-4514 (1991)

[11] Wang, L. V., Wu, H., [Biomedical Optics : Principles and Imaging], Wiley-interscience, Hoboken, 343 (2007)